

# Ultralow lattice thermal conductivity of monolayer penta-silicene and penta-germanene

Zhibin Gao,<sup>\*,†</sup> Zhaofu Zhang,<sup>‡</sup> Gang Liu,<sup>\*,¶</sup> and Jian-Sheng Wang<sup>†</sup>

<sup>†</sup>*Department of Physics, National University of Singapore, Singapore 117551, Republic of Singapore*

<sup>‡</sup>*Department of Engineering, Cambridge University, Cambridge, CB2 1PZ, United Kingdom*

<sup>¶</sup>*School of Physics and Engineering, Henan University of Science and Technology, Luoyang 471023, China*

E-mail: [zhibin.gao@nus.edu.sg](mailto:zhibin.gao@nus.edu.sg); [liugang8105@gmail.com](mailto:liugang8105@gmail.com)

## Abstract

We study the lattice thermal conductivity of two-dimensional (2D) pentagonal systems, such as penta-silicene and penta-germanene. Penta-silicene has been recently reported,<sup>1</sup> while the stable penta-germanene, belonging to the same group IV element, is revealed firstly by our *ab initio* calculations. We find that both penta-silicene and penta-germanene at room temperature have ultralow lattice thermal conductivities  $\kappa$  of 1.29 W/mK and 0.30 W/mK respectively. To the best of our knowledge, penta-germanene may have the lowest  $\kappa$  in 2D crystal materials. We attribute ultralow  $\kappa$  to the weak phonon harmonic interaction and strong anharmonic scattering. A small phonon group velocity, a small Debye frequency, a large Grüneisen parameter, and a large number of modes available for phonon-phonon interplay together lead to the ultralow  $\kappa$  of penta-silicene and penta-germanene. These discoveries provide new insight into the manipulation of ultralow  $\kappa$  in 2D materials and highlight the potential applications of designing silicon and germanium based high thermoelectric materials.<sup>2</sup>

## 1 Introduction

Except for oxygen, silicon is the most abundant element in Earth's crust (27.7%). Since the 1950s, the development of computer technology and the microelectronics industry is based on silicon chips. According to Moore's law, the number of transistors consisting of a chip will be doubled around every 18 months. However, this rule may become deviated due to the tremendous difficulty of scaling down the conventional silicon transistors.<sup>3</sup> Recently, nanomaterials, similar to thin-films, have attracted much attention for more superior transistors.<sup>4</sup>

Silicene, as a representative 2D materials of group IV elements, has been successfully made into field-effect transistors.<sup>5</sup> However, the main drawback for silicene as a transistor material is the absence of a band gap for the on/off ratio.<sup>6</sup> In 2014, penta-graphene with a Cairo pentagonal tiling, as a new carbon allotrope, was firstly predicted and has focused attention on the pentagonal system.<sup>7-10</sup> However, penta-silicene, as a new successor of penta-graphene, has been reported to be unstable due to imaginary frequencies of phonon dispersion.<sup>11,12</sup> Recently, *Guo et al.*<sup>1</sup> proposed that tilting the Si dimers would reduce the Coulomb interaction and stabilize it. Besides, they also reported the strong ferroelectricity with a high Curie temperature of 1190 K

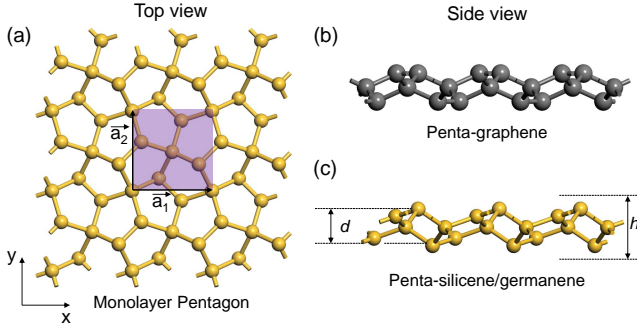


Figure 1: Ball-and-stick model of the 2D pentagonal system of a  $3 \times 3$  supercell in (a) top view (penta-graphene, penta-silicene and penta-germanene). Side views of penta-graphene are shown in (b) and of penta-silicene or penta-germanene are shown in (c). The primitive cell is indicated by the purple shading in (a).  $\vec{a}_1$  and  $\vec{a}_2$  are the corresponding lattice vectors and  $d$  is the buckling distance. The effective thickness  $h$  is defined as the summation of  $d$  and two van der Waals radii of the outmost surface atom of structure.<sup>13</sup>

of penta-silicene. However, a study of the lattice conductivity is lacking. Moreover, it is also interesting to find a stable penta-germanene in group IV element.

In this study, we explore the lattice thermal conductivities and thermal transport properties of penta-silicene and penta-germanene based on *ab initio* calculations. We find that both penta-silicene and penta-germanene have ultralow  $\kappa$  of 1.29 W/mK and 0.30 W/mK at 300 K, which are much lower than the penta-graphene of 645 K. These may be the lowest  $\kappa$  in 2D crystal materials based on our collected data. We attribute both ultralow  $\kappa$  to the weak phonon harmonic interaction and strong anharmonic scattering. We hope these discoveries will make a contribution to the thermal transport of 2D materials and silicon’s energy harvesting power.<sup>2</sup>

## 2 Results and discussion

The optimized structure of the 2D pentagonal system (penta-silicene or penta-germanene) is shown in Figure 1. The top views of penta-graphene and penta-silicene (penta-germanene) are identical and the side views have slightly

difference (distortion).<sup>7</sup> There are 6 atoms in the square primitive cell indicated by the purple shading. Two hybridized types of the chemical bond can be found in this pentagonal system. One is  $sp^3$  with four coordination numbers and the other is  $sp^2$  with three coordination numbers. From another perspective, every 4 pentagons can form a larger 10-sided shape of “boat” in the top view and these pentagons in the side view like a “ladder”. The lattice constants are  $|\vec{a}_1| = |\vec{a}_2| = 3.64 \text{ \AA}$  for penta-graphene,<sup>7</sup>  $|\vec{a}_1| = |\vec{a}_2| = 5.58 \text{ \AA}$  for penta-silicene, and  $|\vec{a}_1| = |\vec{a}_2| = 5.67 \text{ \AA}$  for penta-germanene. According to group theory, regular pentagon, different from the equilateral triangle, quadrangle, and hexagon, can not be periodically arranged in a whole plane. Hence, all 2D pentagon has an intrinsic buckling to keep energetic stability.<sup>14</sup> As the atomic radius increases in group IV element, the buckling distance  $d$  reasonably increases from 1.2  $\text{\AA}$  for penta-graphene<sup>7</sup> to 2.44  $\text{\AA}$  and 3.32  $\text{\AA}$  for penta-silicene and penta-germanene, respectively.

In order to verify the stabilities of penta-silicene and penta-germanene, we calculated the phonon dispersions shown in Figure 2(a) and Figure 2(b). There are 18 phonon branches due to 6 atoms in the primitive cell. Owing to the membrane effect, 2D materials have a linear transverse acoustic (TA), a linear longitudinal acoustic (LA), and a quadratic out-of-plane acoustic (ZA) phonon modes around the  $\Gamma$  point.<sup>15</sup> All phonon frequencies are free from the negative values, indicating dynamical stabilities. Since the averaged phonon frequency is inversely proportional to the atomic mass, the maximum vibrational frequencies are significantly suppressed from the penta-graphene<sup>7</sup> of 1666.5  $\text{cm}^{-1}$  to the penta-silicene of 497.7  $\text{cm}^{-1}$  and finally to the penta-germanene of 250.7  $\text{cm}^{-1}$ , indicating a gradually decreasing trend of the harmonic phonon strength and interatomic bonding.

A large frequency gap between acoustic and optical phonons (*a-o* gap) generally leads to a high lattice thermal conductivity  $\kappa$ ,<sup>16</sup> such as cubic boron arsenide with 2240 W/mK (*a-o* gap  $\approx 306.6 \text{ cm}^{-1}$ )<sup>17</sup> and  $\text{MoS}_2$  with 103

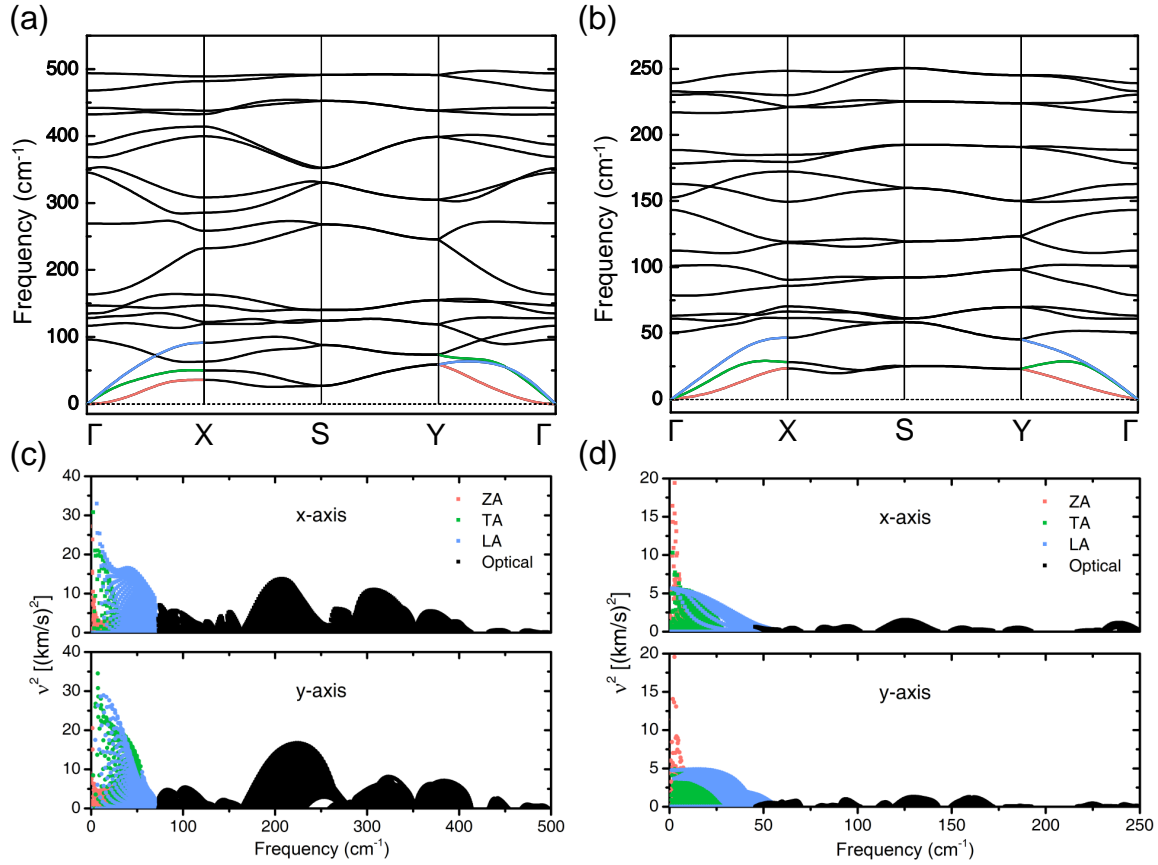


Figure 2: Phonon dispersions of (a) penta-silicene and (b) penta-germanene. In the first Brillouin zone, the high symmetry  $k$  points are:  $\Gamma(0\ 0\ 0)$ ,  $X(1/2\ 0\ 0)$ ,  $S(1/2\ 1/2\ 0)$  and  $Y(0\ 1/2\ 0)$ . Three acoustic phonon branches, which correspond to an out-of-plane (ZA) mode, an in-plane transverse (TA) mode, and an in-plane longitudinal (LA) mode, are marked. Phonon velocity squared of (c) penta-silicene and (d) penta-germanene along x-axis and y-axis with mode resolution.

W/mK ( $a$ - $o$  gap  $\approx 52\text{ cm}^{-1}$ ).<sup>18</sup> From the opposite side, a small  $a$ - $o$  gap is highly desirable for designing ultralow  $\kappa$  materials. The zero  $a$ - $o$  gap is found in Figure 2(a) and Figure 2(b) for penta-silicene and penta-germanene. This implies strong acoustic-optical phonon scattering and ultralow  $\kappa$  in penta-silicene and penta-germanene.<sup>15</sup>

Group velocity, defined by the  $\vec{v} = d\omega/d\vec{q}$ , is one of the key parameters in determining the final  $\kappa$ . Because it is a vector (negative sign represents the opposite direction), we use the scalar  $|\vec{v}|^2$  to study the phonon transport of penta-silicene and penta-germanene with mode resolution along x-axis and y-axis, shown in Figure 2(c) and Figure 2(d). Penta-silicene has a larger  $|\vec{v}|^2$  than penta-germanene no matter along the x-axis and y-axis. Along both of them, larger  $|\vec{v}|^2$  are found in acoustic phonon

modes (colorful dot/cubic) than optical phonon modes (black dot/cubic), indicating a more dispersive behavior of acoustic branches compared to the optical phonon modes. The LA mode of penta-silicene along  $\Gamma$ - $X$  is quite different from that along  $\Gamma$ - $Y$  shown in Figure 2(a) and Figure 2(c), suggesting a large anisotropic phonon property along x-axis and y-axis. However, penta-germanene is almost isotropic shown in Figure 2(b) and Figure 2(d). On the whole, the phonon transport at the group velocity level is significantly suppressed for penta-silicene and penta-germanene compared with the pentagraphene.<sup>19</sup>

In undoped semiconductors and insulators, phonons, rather than electrons, are the main carrier for the heat transport. In the framework of relaxation time approximation (RTA) and Boltzmann equation, lattice thermal con-

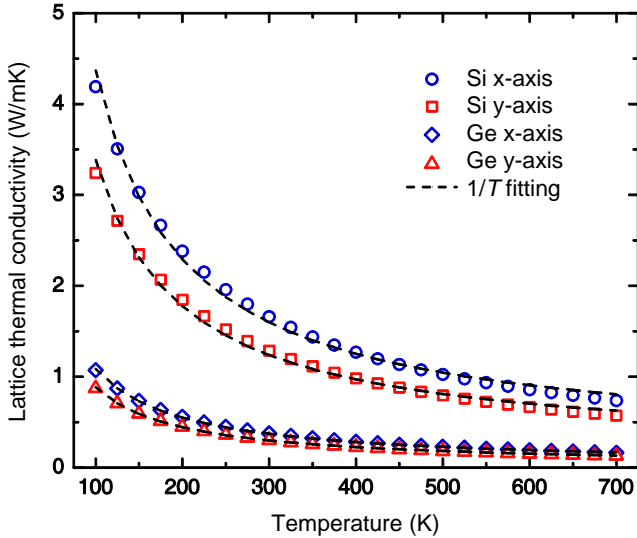


Figure 3: Lattice thermal conductivity of penta-silicene and penta-germanene as a function of temperature along x-axis and y-axis from the Boltzmann transport equation.  $1/T$  fittings are shown in the dashed lines, indicating a dominant Umklapp process of phonon-phonon scattering that brings about the thermal resistivity.

ductivity  $\kappa$  with phonon modes  $\lambda$  and wave vector  $\mathbf{q}$  can be obtained:<sup>15</sup>

$$\kappa_{\alpha\beta} = \frac{1}{V} \sum_{\lambda} C_{\lambda} v_{\lambda\alpha} v_{\lambda\beta} \tau_{\lambda}, \quad (1)$$

in which  $V$  is the volume of the primitive cell,  $C_{\lambda}$ ,  $\tau_{\lambda}$ , and  $v_{\lambda\alpha}$  are the specific heat, relaxation time, and group velocity in the Cartesian direction  $\alpha$  of each single phonon mode  $\lambda$  ( $\nu$ ,  $\mathbf{q}$ ), respectively. Generally, there are two types of phonon-phonon scattering. One is the Umklapp (U) process and the other is the Normal (N) process. The former is the only contributor to thermal resistance. To solve the single-mode RTA equation, the N process can not be excluded from the whole scattering rates and is wrongly regarded as same as the U process. Hence, we use the corrected result after adopting iterative procedure (removal of the N process).<sup>20,21</sup>

Figure 3 shows the calculated  $\kappa$  of penta-silicene and penta-germanene along the x-axis and y-axis. Although the lattice constants along the x-axis and y-axis are the same,

the  $\kappa$  values of heat transport are obviously anisotropic. At room temperature,  $\kappa$  of penta-silicene are 1.66 W/mK along the x-axis and 1.29 W/mK along the y-axis. For penta-germanene, the  $\kappa$  are reduced to 0.38 W/mK and 0.30 W/mK along both directions, implying a strong anisotropic heat transport property. This is quite different from that of penta-graphene which has an isotropic  $\kappa$  of 645 W/mK at 300 K.<sup>19</sup> The anisotropy ratio ( $\kappa_x/\kappa_y$ ) is 1.29 for penta-silicene and 1.25 for penta-germanene, respectively. This phenomenon can be derived from the anisotropic phonon dispersions and phonon group velocities shown in Figure 2. This in-plane anisotropic property may attract more attention to orientation-dependent thermal devices<sup>22</sup> and increase the diversity of the 2D pentagonal system in group IV elements.

Table 1: Relevant thermal properties of silicon and germanium based 2D materials, as well as penta-graphene.  $\omega_D^a$  (THz),  $\omega_{\Gamma}^o$  (THz) and  $\kappa$  (W/mK) are the largest acoustic phonon frequency (Debye frequency), lowest optical phonon frequency at  $\Gamma$  point and lattice thermal conductivity at 300 K, respectively. All intrinsic  $\kappa$  is the smaller one if the material is anisotropic along x and y directions.

Materials	$\omega_D^a$	$\omega_{\Gamma}^o$	$\kappa$
Silicene <sup>a</sup>	6.00	5.70	9.40
Germanene <sup>b</sup>	2.91	5.10	2.38
SiTe <sub>2</sub> <sup>c</sup>	2.77	2.34	2.27
Penta-C <sup>d</sup>	14.8	17.5	645
Penta-Si <sup>e</sup>	3.01	2.89	1.29
Penta-Ge <sup>e</sup>	1.75	1.52	0.30

<sup>a</sup> Hexagonal silicene.<sup>23</sup> <sup>b</sup> Hexagonal germanene.<sup>24</sup> <sup>c</sup> 1T-SiTe<sub>2</sub>.<sup>25</sup> <sup>d</sup> Penta-graphene.<sup>7</sup> <sup>e</sup> Present work.

According to the Slack model for bulk materials, there are two vital parameters correlated with  $\kappa$ . One is the largest acoustic phonon frequency (Debye frequency)  $\omega_D^a$ , and the other one is the Grüneisen parameter  $\gamma$ .<sup>26</sup> Long-wave (acoustic) phonons are the main contributors to

the heat transport. A low  $\omega_D^a$ , usually, means a small  $\kappa$ . The calculated  $\omega_D^a$  are shown in Table 1. In order to compare, we also list other silicon and germanium based 2D materials. Silicene and germanene are the representatives of hexagonal lattice and SiTe<sub>2</sub> belongs to TMDs<sup>27</sup> and is regarded as a superior thermoelectric material.<sup>25,28</sup> Based on Table 1, we can find that  $\kappa$  is proportional to the  $\omega_D^a$ , verifying the correctness of the Slack model prediction in 2D materials qualitatively.

More importantly, penta-silicene and penta-germanene have the lowest  $\kappa$  in all silicon and germanium based 2D materials. Based on our previous collection,<sup>15</sup> penta-germanene has the smallest  $\kappa$  of 0.30 W/mK in the 2D family. This ultralow  $\kappa$  is highly desirable for the ultrahigh thermoelectric material since  $\kappa$  is inversely proportional to the efficiency of conversion from the heat energy to the electrical energy.<sup>29</sup> Besides, as temperature increases,  $\kappa$  decreases significantly for the pentagonal system. The  $\kappa$  can be well described by  $\kappa \propto 1/T$ , indicating the dominant phonon-phonon Umklapp scattering in penta-silicene and penta-germanene. As temperature increases to 600 K,  $\kappa$  is further suppressed to 0.86 W/mK and 0.66 W/mK along the x-axis and y-axis for penta-silicene, while they are 0.19 W/mK and 0.15 W/mK for penta-germanene.

According to the Eq. (1) and the Slack model, anharmonic phonon property also has a large effect on thermal transport and  $\kappa$ . Specifically, the phonon relaxation time relies on two components: (i) the intensity of each phonon-phonon scattering mode. This quantity can be reflected by the mode-dependent Grüneisen parameter  $\gamma$  which is defined as<sup>8</sup>

$$\gamma = -\frac{d \ln \omega}{d \ln V}, \quad (2)$$

where phonon frequency  $\omega$  is a function of band indexes  $\nu$ , and wave vector  $\mathbf{q}$ . (ii) the total number of phonon-phonon scattering modes. Each available phonon scattering mode must simultaneously satisfy the energy and quasi-momentum conservations. This process can be quantitatively described by the volume of the

scattering phase space  $P_3$  for three-phonon processes.<sup>30,31</sup> These two parameters finally enter into the three-phonon scattering rates, written as

$$\Gamma_{\lambda\lambda'\lambda''}^+ = \frac{\hbar\pi}{4} \frac{f_0' - f_0''}{\omega_\lambda \omega_{\lambda'} \omega_{\lambda''}} |V_{\lambda\lambda'\lambda''}^+|^2 \delta(\omega_\lambda + \omega_{\lambda'} - \omega_{\lambda''}), \quad (3)$$

$$\Gamma_{\lambda\lambda'\lambda''}^- = \frac{\hbar\pi}{4} \frac{f_0' + f_0'' + 1}{\omega_\lambda \omega_{\lambda'} \omega_{\lambda''}} |V_{\lambda\lambda'\lambda''}^-|^2 \delta(\omega_\lambda - \omega_{\lambda'} - \omega_{\lambda''}), \quad (4)$$

where  $\Gamma_{\lambda\lambda'\lambda''}^+$  and  $\Gamma_{\lambda\lambda'\lambda''}^-$  stand for the absorption and emission processes.<sup>20</sup> The Grüneisen parameter  $\gamma$  is proportional to the scattering matrix elements  $|V_{\lambda\lambda'\lambda''}^\pm|$  and the number of Dirac delta distributions is equal to  $P_3$ . We can find that three-phonon scattering rates  $\Gamma_{\lambda\lambda'\lambda''}$  are closely positive correlated with  $\gamma$  and  $P_3$ . We will discuss the anharmonic phonon behavior of the 2D pentagonal system from the above two important factors.

According to the Eq. (2),  $\gamma$  provides the anharmonic phonon property and a large  $\gamma$  means a large anharmonicity. The calculated  $\gamma$  of penta-silicene and penta-germanene with mode resolution is shown in Figure 4. It is found that acoustic phonon modes for both materials have large negative  $\gamma$ , while optical phonon branches have small positive  $\gamma$ . Like graphene, a negative sign of  $\gamma$ , generally implies a negative thermal expansion that will mitigate the thermal strain and stress in high-temperature electronic devices.<sup>32,33</sup> Based on the previous work,  $\gamma$  of ZA mode for penta-graphene is large, however,  $\gamma$  of TA and LA phonon modes are quite small (around zero).<sup>19</sup> This situation is different from that of penta-silicene and penta-germanene.  $\gamma$  of TA mode in penta-silicene (green dot) has the averaged value of around  $-10$  but smaller than that of penta-germanene with an averaged value of around  $-15$  (green cubic). From this angle, penta-germanene has the largest anharmonic interactions with mode resolution in the 2D pentagonal system.

The calculated  $P_3$  of penta-silicene and penta-germanene are shown in Figure 4(c) and Figure 4(d). Evidently,  $P_3$  of penta-germanene is larger than that of penta-silicene, indicat-

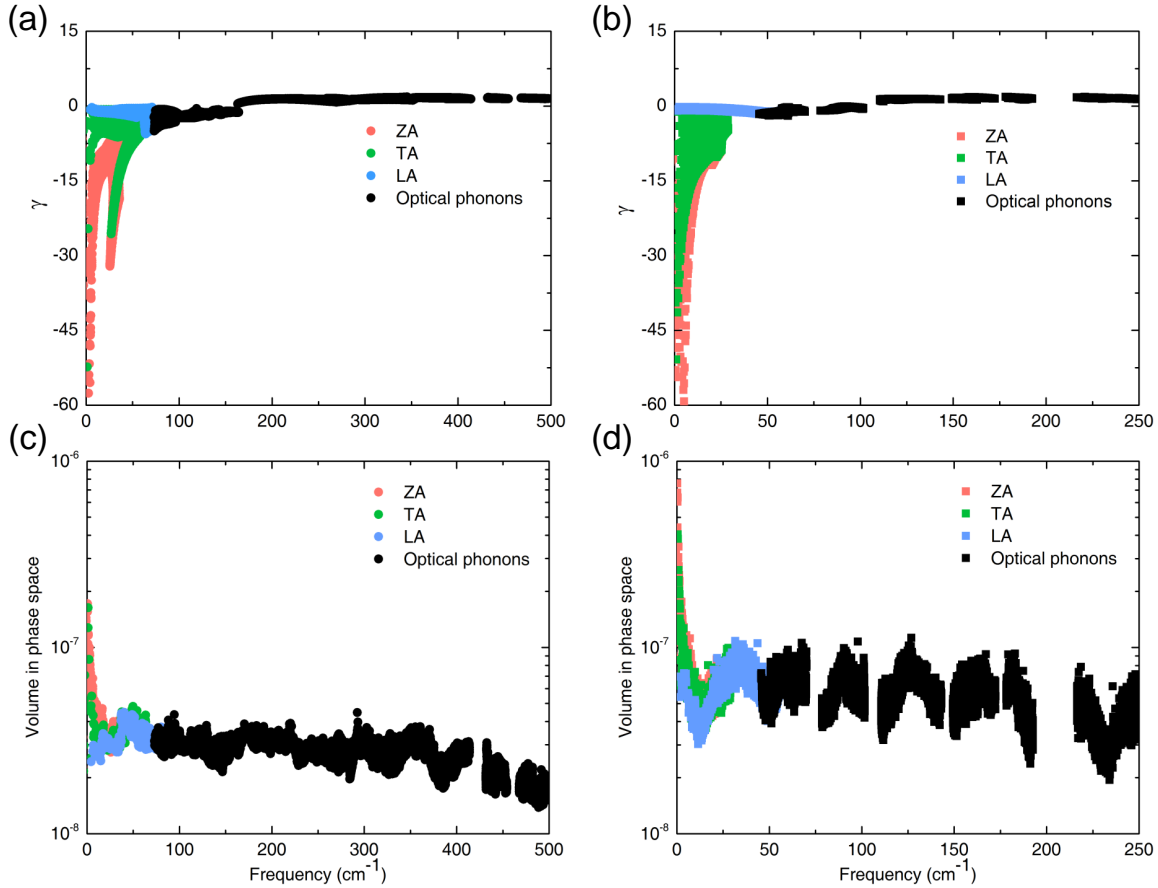


Figure 4: The Grüneisen parameter  $\gamma$  of (a) penta-silicene and (b) penta-germanene as a function of the phonon frequency with mode resolution. Phase-space volume  $P_3$  for three-phonon anharmonic scattering process of (c) penta-silicene and (d) penta-germanene.  $P_3$  is inversely proportional to the lattice thermal conductivity  $\kappa$  qualitatively.

ing a larger number of phonon-phonon scattering channels.  $P_3$  of penta-silicene is smaller than that of penta-graphene.<sup>19</sup> Therefore, we can conclude that the difference of  $\kappa$  between penta-silicene and penta-graphene originates from the Grüneisen parameter  $\gamma$  and group velocity  $v$ , rather than the volume in phase space  $P_3$ . Specifically, a larger  $\gamma$ , a larger  $P_3$ , and a smaller  $v$  lead to a smaller  $\kappa$  of penta-germanene compared to the penta-silicene.

The above two independent factors ( $\gamma$  and  $P_3$ ) finally lead to one vital parameter called three-phonon scattering rates (reciprocal of the relaxation time) shown in Eq. (3) and Eq. (4). This quantity directly enters the  $\kappa$  shown in Eq. (1). A large anharmonic scattering rate needs a large  $\gamma$  and  $P_3$  concurrently. The calculated anharmonic scattering rates of penta-silicene and penta-germanene are shown in Figure 5(a) and Figure 5(b). Overall, the anharmonic scatter-

ing rates of both are comparable. However, the anharmonic scattering rates of LA mode in Figure 5(a) in penta-silicene are quite larger than that of penta-germanene Figure 5(b). There is an interesting region of large acoustic-optical phonon scattering located from 40  $\text{cm}^{-1}$  to 90  $\text{cm}^{-1}$  in penta-silicene, indicating strong phonon-phonon interactions between acoustic phonons and optical phonons. This originates the special phonon dispersion shown in Figure 2(a). Compared with the penta-germanene, penta-silicene has a larger cross-region between acoustic phonons and optical phonons, which makes more easier to simultaneously satisfy the energy and quasi-momentum conservations.

To further explore the underlying phonon scattering mechanism, we plot the mode contribution of three acoustic phonons to the  $\kappa$  for penta-silicene and penta-germanene shown in Figure 5(c) and Figure 5(d). Only two types

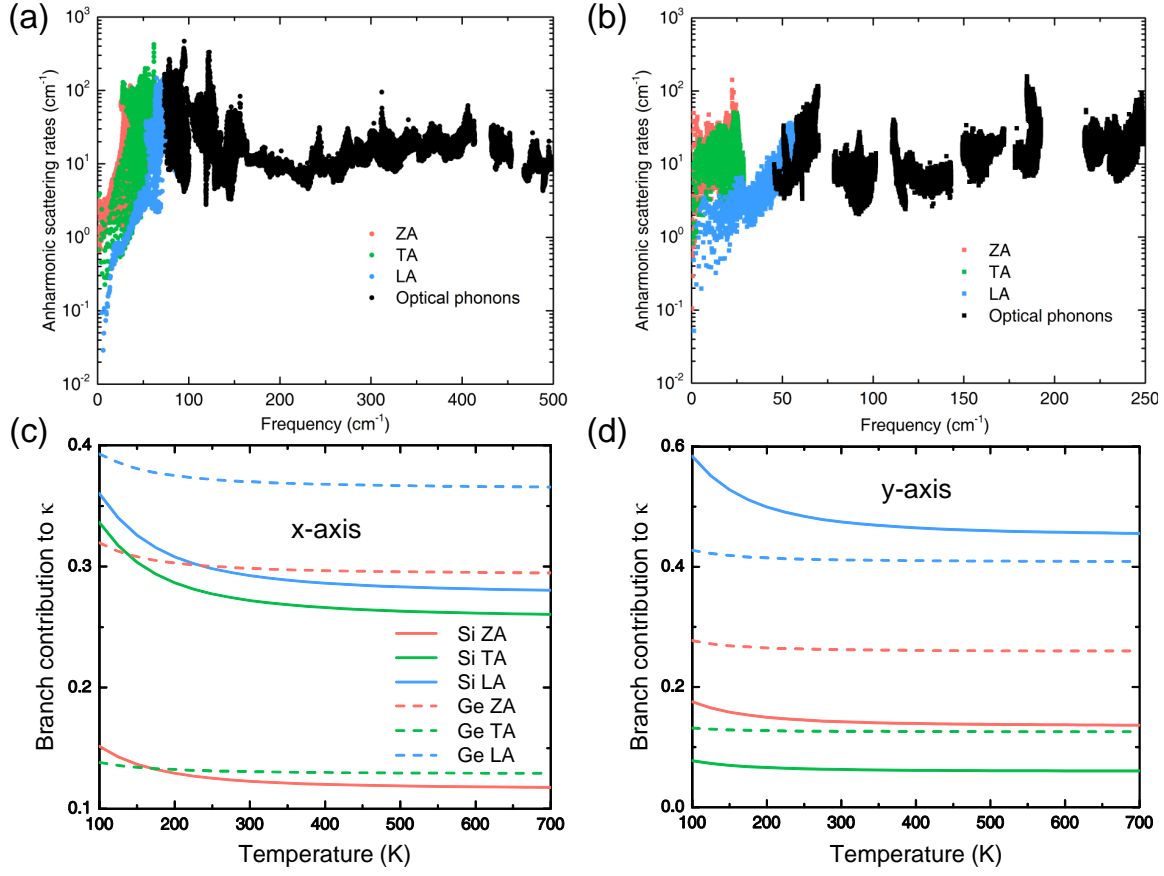


Figure 5: Calculated anharmonic scattering rates of (a) penta-silicene and (b) penta-germanene with mode resolution at 300 K. The normalized contribution of three acoustic phonon branches to the lattice thermal conductivity  $\kappa$  along the (c) x-axis and (d) y-axis as a function temperature.

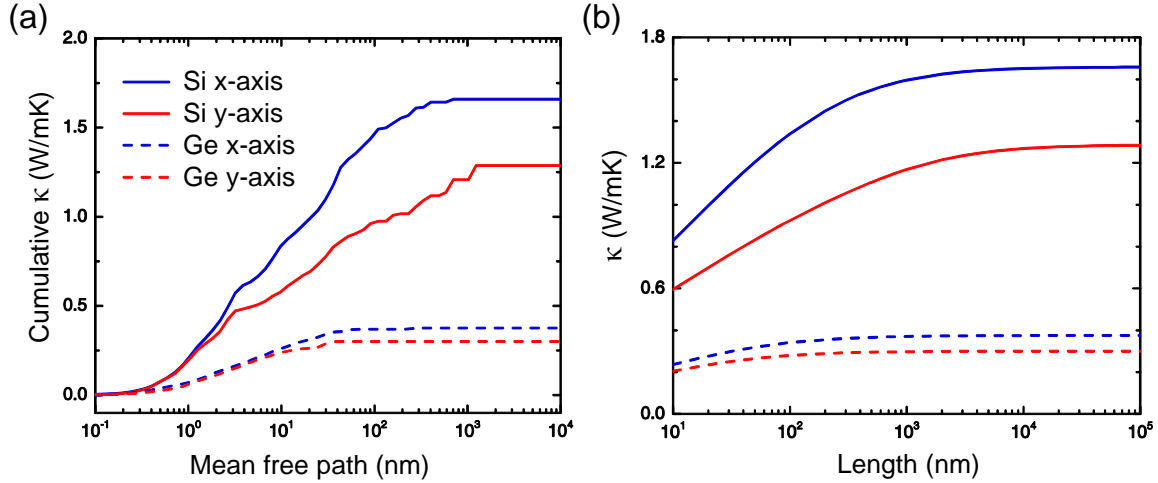


Figure 6: (a) The cumulative lattice thermal conductivity  $\kappa$  as a function of the phonon mean free path of penta-silicene (solid lines) and penta-germanene (dashed lines) along x-axis and y-axis at 300 K. (b)  $\kappa$  as a function of sample size based on the Eq. (6) at 300 K.

of scattering processes are allowed here. One is the scattering within three acoustic phonons and the other one is the scattering between two acoustic phonons (one acoustic phonon

and one optical phonon (two optical phonons). In x-axis, LA and TA modes dominate the heat transport and ZA mode only contributes around 12.5% in penta-silicene at 300 K. For

penta-germanene, LA mode contributes 38% and ZA mode contributes 30% to the  $\kappa$  at the same temperature. This is quite different from that in graphene where 75%  $\kappa$  originates from the ZA phonon mode.<sup>34</sup> In the y-axis, the situation is a little different. LA mode still contributes most to the  $\kappa$  in both materials while the TA's contribution is quite small. This anisotropic property of phonon mode contribution can be traced back to the anisotropic phonon group velocity shown in Figure 2.

Furthermore, we also evaluate the cumulative  $\kappa$  with respect to the phonon mean free path for both penta-silicene and penta-germanene along x and y-axis at 300 K shown in Figure 6(a). In order to obtain the characteristic length  $l_0$ , we use a single parametric function<sup>20</sup>

$$\kappa(l \leq l_{max}) = \frac{\kappa_0}{1 + l_0/l_{max}}, \quad (5)$$

in which  $l_0$  is the only parameter to be determined.  $l_{max}$  and  $\kappa_0$  are the maximum mean free path and ultimately cumulative  $\kappa$ . The calculated cumulative  $\kappa$  of penta-silicene and penta-germanene are shown in Figure 6. The fitted parameters, for penta-silicene are 9.95 nm and 13.69 nm along the x-axis and y-axis. Similarly,  $l_0$  are 4.18 nm and 3.23 nm for penta-germanene along both directions. This characteristic length  $l_0$  can be regarded as a representative mean free path of materials. A low  $l_0$  means a low mean free path of phonon-phonon scattering. Due to Moore's Law, the size of the electronic devices is still decreasing and the role of heat transport in these nanomaterials is becoming increasingly more crucial to modern transistors. Besides,  $l_0$  can be evaluated the different types of phonon behavior such as ballistic transport, diffusive transport, superdiffusive transport, and hydrodynamics.<sup>35-38</sup> In penta-graphene,  $l_0$  equals 278 nm when cumulative  $\kappa$  reaches 50% of the total  $\kappa$ ,<sup>19</sup> while the values of  $l_0$  reduced significantly to 14.2 nm for penta-silicene and 3.2 nm for penta-germanene along the y-axis, respectively. Furthermore, the  $\kappa$  of penta-silicene and penta-germanene can be further suppressed by inducing the phonon-boundary scattering and isotope effect scatter-

ing.

In reality, electronic devices must have a length scale. Hence, scattering between boundary and phonons becomes a very important factor in thermal transport at the nanoscale. Specifically, the boundary scattering has been well described and verified in 2D materials, such as in graphene.<sup>39</sup> The semi-empirical formula can be written as<sup>39,40</sup>

$$\frac{1}{\tau_b} = \frac{v_{\nu q}}{L}, \quad (6)$$

in which  $L$  and  $v_{\nu q}$  represent the material size and phonon group velocity. This part of the scattering rate will be added to the phonon-phonon scattering rate using the Matthiessen's rule  $1/\tau_{total} = 1/\tau_{p-p} + 1/\tau_b$ .<sup>41</sup> The calculated  $\kappa$  of penta-silicene and penta-germanene as a function of sample length  $L$  are shown in Figure 6(b). As  $L$  decreases from 100 nm to 10 nm, the  $\kappa$  reduces following an exponential function  $\kappa \propto \log L$  due to the strong boundary effect, which has been experimentally verified in suspended graphene in 2014.<sup>42</sup>

For an instance, when  $L$  is equal to 1  $\mu\text{m}$ , the  $\kappa$  of penta-silicene are reduced to 1.59 W/mK and 1.17 W/mK along the x and y-axis, while the  $\kappa$  of penta-germanene are suppressed to 0.37 W/mK and 0.29 W/mK along both directions. When  $L$  equals 100 nm, the  $\kappa$  of penta-silicene has 80% and 72% percents along the x and y-axis compared with the  $\kappa$  of material with infinite size. Similarly, the  $\kappa$  of penta-germanene has 90% and 93% percents along x and y-axis. In this sense, the  $\kappa$  of penta-silicene is more sensitive to the sample length  $L$  with respect to the penta-germanene. The reason is that, for an instance, the characteristic lengths  $l_0$  of penta-silicene and penta-germanene are 14.2 nm and 3.2 nm along the y-axis. Hence, at the same length (for example, 1  $\mu\text{m}$ ), more phonons can be scattering by the boundary in penta-silicene than that of penta-germanene.

We also calculate the electronic thermal conductivity based on the Wiedemann-Franz law, we find that electronic thermal conductivity is much lower than lattice thermal conductivity and can be neglected for low concentration doping ( $n_i 10^{12} \text{ cm}^{-2}$ ). As the carrier concentra-

tion doping increases, the electronic conductivity increases and electronic thermal conductivity increases simultaneously ( $10^{12} \text{ cm}^{-2}$ ,  $n_i 10^{13} \text{ cm}^{-2}$ ) due to the population enhancement. For a much higher concentration doping ( $n_i 10^{13} \text{ cm}^{-2}$ ), both materials behavior like a good “metal” having free carriers. Hence, electronic thermal conductivity increases significantly as a function of carrier concentration.

### 3 Conclusion

In summary, based on the *ab initio* calculations and the Boltzmann equation, we have, firstly, obtained the lattice thermal conductivities and thermal transport properties of penta-silicene and penta-germanene, belonging to the 2D pentagonal system in group IV element. We have found that the lattice thermal conductivities of penta-silicene and penta-germanene are 1.29 W/mK and 0.30 W/mK, respectively, which are much smaller than that of penta-graphene of 645 W/mK at room temperature.<sup>19</sup> More importantly, penta-germanene, to the best of our knowledge, may have the lowest lattice thermal conductivity in 2D crystal materials by far.<sup>15</sup> It could be favorable if this prediction can be further confirmed by other independent methods, such as molecular dynamics. This ultralow lattice thermal conductivity can be traced to low phonon harmonic interaction and strong anharmonic scattering. A small phonon group velocity and a small Debye frequency indicate a weak phonon harmonic interaction. A large Grüneisen parameter implies a strong phonon scattering per each phonon mode and a big volume in phase space means a large number modes available for phonon-phonon interplay. Together these parameters finally lead to the ultralow lattice thermal conductivity of penta-silicene and penta-germanene in the 2D pentagonal system.

Although penta-silicene and penta-germanene are metastable structures, penta-silicene nanoribbon has been successfully synthesized in 2016 and has shown exotic phenomena, such as topologically protected phases or increased spin-orbit effects.<sup>43,44</sup> Besides, previ-

ous work also theoretically verified that penta-silicene can be stably grown on the Ag surface,<sup>1</sup> which means a proper confining material (e.g., a metal substrate) is needed to produce the titled penta-silicene and penta-germanene in experiments. In this sense, we hope more experimentalists could make attempts on the 2D pentagonal system such as by using the reactive molecular beam epitaxy method.<sup>45</sup> The ultralow thermal conductivity of penta-silicene and penta-germanene may make a contribution to the thermal transport of 2D materials and silicon’s energy harvesting power.<sup>2</sup>

### 4 Computational method

The equilibrium geometry and structural stability were calculated by density functional theory (DFT) implemented in the VASP code.<sup>46,47</sup> The exchange-correlation functional of Perdew-Burke-Ernzerhof (PBE)<sup>48</sup> was used. A plane-wave cutoff energy of 500 eV was adopted and a Monkhorst-Pack Brillouin zone was sampled by  $11 \times 11$ . The total energy threshold and Hellmann-Feynman forces between adjacent optimization were  $10^{-6}$  eV and  $10^{-3}$  eV/Å. To eliminate spurious interactions between periodic slabs, a vacuum separation distance of 20 Å was applied. Phonon frequency was calculated in Phonopy<sup>49</sup> with a  $5 \times 5$  supercell. Anharmonic interatomic force constants (IFCs) were extracted in ShengBTE<sup>20</sup> by solving the linearized Boltzmann transport equation. The converged  $\kappa$  was obtained after careful parameter testing. The interaction cutoff was 0.55 nm and the  $\Gamma$ -centered q-grid was  $101 \times 101$ . A scale broadening parameter of 0.1 for Gaussian smearing was used. Since thickness for 2D material is not well-defined, an effective thickness should be chosen to compare with the 3D material. Here, the effective thickness  $h$  is defined as the summation of buckling distance  $d$  and two van der Waals radii of the outmost surface atom of structure.<sup>13,50</sup> For penta-silicene and penta-germanene,  $d$  are 2.44 Å and 3.32 Å, while  $h$  are 6.64 Å and 7.54 Å, respectively.

## Conflicts of interest

There are no conflicts to declare.

## Author Information

### ORCID

Zhibin Gao: 0000-0002-6843-381X

Zhaofu Zhang: 0000-0002-1406-1256

## Acknowledgements

We thank Jiongzhi Zheng for helpful discussions. This work is supported by an MOE tier 1 grant R-144-000-402-114.

## References

- (1) Y. Guo, C. Zhang, J. Zhou, Q. Wang and P. Jena, *Phys. Rev. Applied*, 2019, **11**, 064063.
- (2) G. Hu, H. Edwards and M. Lee, *Nat. Electron.*, 2019, **2**, 300–306.
- (3) N. Mathur, *Nature*, 2002, **419**, 573.
- (4) A. D. Franklin, *Science*, 2015, **349**, aab2750.
- (5) G. Le Lay, *Nat. Nanotechnol.*, 2015, **10**, 202.
- (6) S. Cahangirov, M. Topsakal, E. Aktürk, H. Şahin and S. Ciraci, *Phys. Rev. Lett.*, 2009, **102**, 236804.
- (7) S. Zhang, J. Zhou, Q. Wang, X. Chen, Y. Kawazoe and P. Jena, *Proc. Natl. Acad. Sci. U. S. A.*, 2015, **112**, 2372–2377.
- (8) X. Wu, V. Varshney, J. Lee, T. Zhang, J. L. Wohlwend, A. K. Roy and T. Luo, *Nano Lett.*, 2016, **16**, 3925–3935.
- (9) H. Liu, G. Qin, Y. Lin and M. Hu, *Nano Lett.*, 2016, **16**, 3831–3842.
- (10) A. D. Oyedele, S. Yang, L. Liang, A. A. Puretzky, K. Wang, J. Zhang, P. Yu, P. R. Pudasaini, A. W. Ghosh, Z. Liu, C. M. Rouleau, B. G. Sumpter, M. F. Chisholm, W. Zhou, P. D. Rack, D. B. Geohegan and K. Xiao, *J. Am. Chem. Soc.*, 2017, **139**, 14090–14097.
- (11) Y. Ding and Y. Wang, *J. Mater. Chem. C*, 2015, **3**, 11341–11348.
- (12) Y. Aierken, O. Leenaerts and F. M. Peeters, *Phys. Chem. Chem. Phys.*, 2016, **18**, 18486–18492.
- (13) Z. Gao, X. Dong, N. Li and J. Ren, *Nano Lett.*, 2017, **17**, 772–777.
- (14) E. Ressouche, V. Simonet, B. Canals, M. Gospodinov and V. Skumryev, *Phys. Rev. Lett.*, 2009, **103**, 267204.
- (15) Z. Gao, F. Tao and J. Ren, *Nanoscale*, 2018, **10**, 12997–13003.
- (16) S. Li, Q. Zheng, Y. Lv, X. Liu, X. Wang, P. Y. Huang, D. G. Cahill and B. Lv, *Science*, 2018, **361**, 579–581.
- (17) L. Lindsay, D. A. Broido and T. L. Reinecke, *Phys. Rev. Lett.*, 2013, **111**, 025901.
- (18) Y. Cai, J. Lan, G. Zhang and Y.-W. Zhang, *Phys. Rev. B: Condens. Matter Mater. Phys.*, 2014, **89**, 035438.
- (19) F. Q. Wang, J. Yu, Q. Wang, Y. Kawazoe and P. Jena, *Carbon*, 2016, **105**, 424–429.
- (20) W. Li, J. Carrete, N. A. Katcho and N. Mingo, *Comput. Phys. Commun.*, 2014, **185**, 1747–1758.
- (21) L. Lindsay, D. A. Broido and T. L. Reinecke, *Phys. Rev. B: Condens. Matter Mater. Phys.*, 2013, **87**, 165201.
- (22) Y. Du, J. Maassen, W. Wu, Z. Luo, X. Xu and P. D. Ye, *Nano Lett.*, 2016, **16**, 6701–6708.
- (23) H. Xie, M. Hu and H. Bao, *Appl. Phys. Lett.*, 2014, **104**, 131906.

- (24) B. Peng, H. Zhang, H. Shao, Y. Xu, G. Ni, R. Zhang and H. Zhu, *Phys. Rev. B: Condens. Matter Mater. Phys.*, 2016, **94**, 245420.
- (25) Y. Wang, Z. Gao and J. Zhou, *Physica E*, 2019, **108**, 53–59.
- (26) G. A. Slack, *J. Phys. Chem. Solids*, 1973, **34**, 321–335.
- (27) Z. Gao, Z. Zhou and D. Tománek, *ACS Nano*, 2019, **13**, 5103–5111.
- (28) V. Tshitoyan, J. Dagdelen, L. Weston, A. Dunn, Z. Rong, O. Kononova, K. A. Persson, G. Ceder and A. Jain, *Nature*, 2019, **571**, 95–98.
- (29) Z. Gao, G. Liu and J. Ren, *ACS Appl. Mater. Interfaces*, 2018, **10**, 40702–40709.
- (30) L. Lindsay and D. Broido, *J. Phys.: Condens. Matter*, 2008, **20**, 165209.
- (31) S. Lee, K. Esfarjani, T. Luo, J. Zhou, Z. Tian and G. Chen, *Nat. Commun.*, 2014, **5**, 3525.
- (32) G. Liu, Z. Gao and J. Ren, *Phys. Rev. B: Condens. Matter Mater. Phys.*, 2019, **99**, 195436.
- (33) G. Liu, Z. Gao and J. Zhou, *Physica E*, 2019, **112**, 59–65.
- (34) L. Lindsay, D. A. Broido and N. Mingo, *Phys. Rev. B: Condens. Matter Mater. Phys.*, 2010, **82**, 115427.
- (35) S. Lee, D. Broido, K. Esfarjani and G. Chen, *Nat. Commun.*, 2015, **6**, 6290.
- (36) A. Cepellotti, G. Fugallo, L. Paulatto, M. Lazzeri, F. Mauri and N. Marzari, *Nat. Commun.*, 2015, **6**, 6400.
- (37) Z. Gao, N. Li and B. Li, *Phys. Rev. E*, 2016, **93**, 022102.
- (38) Z. Gao, N. Li and B. Li, *Phys. Rev. E*, 2016, **93**, 032130.
- (39) A. A. Balandin, S. Ghosh, W. Bao, I. Calizo, D. Teweldebrhan, F. Miao and C. N. Lau, *Nano Lett.*, 2008, **8**, 902–907.
- (40) D. Nika, E. Pokatilov, A. Askerov and A. Balandin, *Phys. Rev. B: Condens. Matter Mater. Phys.*, 2009, **79**, 155413.
- (41) J. S. Kang, M. Ke and Y. Hu, *Nano Lett.*, 2017, **17**, 1431–1438.
- (42) X. Xu, L. F. C. Pereira, Y. Wang, J. Wu, K. Zhang, X. Zhao, S. Bae, C. Tinh Bui, R. Xie, J. T. L. Thong, B. H. Hong, K. P. Loh, D. Donadio, D. Donadio and B. Özyilmaz, *Nat. Commun.*, 2014, **5**, 3689.
- (43) J. I. Cerdá, J. Sławińska, G. Le Lay, A. C. Marele, J. M. Gómez-Rodríguez and M. E. Dávila, *Nat. Commun.*, 2016, **7**, 13076.
- (44) G. Prévot, C. Hogan, T. Leoni, R. Bernard, E. Moyen and L. Masson, *Phys. Rev. Lett.*, 2016, **117**, 276102.
- (45) D. Ji, S. Cai, T. R. Paudel, H. Sun, C. Zhang, L. Han, Y. Wei, Y. Zang, M. Gu and Y. Zhang, *Nature*, 2019, **570**, 87.
- (46) G. Kresse and J. Furthmüller, *Phys. Rev. B: Condens. Matter Mater. Phys.*, 1996, **54**, 11169–11186.
- (47) G. Kresse and J. Furthmüller, *Comput. Mater. Sci.*, 1996, **6**, 15–50.
- (48) J. P. Perdew, K. Burke and M. Ernzerhof, *Phys. Rev. Lett.*, 1996, **77**, 3865–3868.
- (49) A. Togo, F. Oba and I. Tanaka, *Phys. Rev. B: Condens. Matter Mater. Phys.*, 2008, **78**, 134106.
- (50) Z. Gao, D. Liu and D. Tománek, *Physical Review Applied*, 2018, **10**, 064039.